HEAT TRANSFER THROUGH POROUS MEDIA IN THE COUNTERFLOW REGIME OF HE II

R. Maekawa*, B. Baudouy

CEA/Saclay, DSM/DAPNIA/SACM
91191 Gif-sur-Yvette Cedex, France

ABSTRACT

Experimental results are presented for He II counter flow regime through Al_2O_3 porous media. Tests have been performed on three porous disks with different thicknesses, 2, 3 and 4 mm, having the same porosity of 32 %, average pore diameter of 2 μm and permeability in the range of 10^{-14} m^2. Temperature and pressure differences have been measured across porous media from 1.4 K to 2.1 K in the saturated superfluid helium. The influence on the porous media thickness to the heat transfer is clearly seen on the typical linear Darcy regime and the turbulent Gorter-Mellink regime. Deviation from these classical laws is observed for large temperature difference that can be attributed to the change of He II heat transfer properties due to the complex flow paths of porous media. The effect of porous media thickness to the He II heat transfer is discussed.

INTRODUCTION

With the renewed interest of the use of Nb_3Sn superconductor for high field magnet for the next Hadron collider generation currently under study, engineers are developing new electrical insulation system. For this next generation of magnet, ceramic materials are investigated as possible candidate for the electrical insulation system for the magnet winding [1]. Ceramic insulation with good wrapping capability and excellent thermal resistance during the heat treatment would eliminate complex coil fabrication, lower costs and reduce fabrication time. For magnets cooled by superfluid helium, the thermal resistance created by the conventional electrical insulation of the cables forms the main thermal resistance to He II cooling [2]. Ceramic materials can have porosities much lower than conventional electrical insulation, which would reduce even more cooling efficiency with helium. A joint program between NIFS and CEA/ Saclay had been launched to study

* On leave from NIFS, Toki Gifu, Japan

FIGURE 1. The binary image of the sample: white heat transfer area and black glued area. From the right hand side, 2mm, 3mm and 4mm sample. The heat transfer area is attributed to the white area.

thermal behavior of porous media, extensively. Further, the study is concentrated on the large heat fluxes and temperatures variation, the critical and the maximum heat fluxes on different samples of the same porous media kind having different thicknesses.

DESCRIPTION OF EXPERIMANTAL SET-UPS AND SAMPLES

Porous Media Samples

The porous samples used in this study are constituted with over 97% of Al_2O_3 and have been purchased from Krosaki Harima. We studied three samples having the same geometrical properties with three different thicknesses 2, 3 and 4 mm, respectively. Samples have a 2 mm average pore and a porosity of 32%. The properties are presented in TABLE 1. For the experiments, a stainless steel support flange is machined to hold the porous sample. The DP-190 was used to seal the porous disk to the stainless steel interface to avoid any heat leak through the imperfect seal. In addition, G-10 sheet is glued on the sample to match the heat transfer area on the both sides. Since parts of glue penetrate to the heat transfer area, the both sides of the sample are scanned with a scanner with 1024 dpi image. The image is them converted to a binary mode as shown in FIGURE 1. The software counts these pixels to determine heat transfer area of the sample. The results of cross section measurements are presented in TABLE 2.

Helium II Heat Transfer Measurement

FIGURE 2 shows a schematic of experimental set-up. The apparatus consists of two stainless steel cylindrical vacuum cans, creating a thermal insulation space between the test section (the inner vacuum can) and the surrounding He II bath. The diameter and the height of the test section are 72 mm and 31 mm, respectively. Indium wire, 1.6 mm diameter, is utilized as an o-ring to assemble the support flange and the two vacuum cans. 12 stainless steel bolts, equally spaced around the circumference of the flange, are tightened equally to apply compression to the o-rings and ensure helium leak. The whole apparatus is immersed in the saturated He II bath for the experiment.

TABLE 1. Properties of the Porous Media.

Thickness (mm)	2	3	4
Average Pore diameter (μm)	2	2	2
Density (g/cm^3)	2.68	2.68	2.68
Porosity (%)	32	32	32
Average Permeability $\times 10^{14}$ (m^2) Given by Krosaki Harima	1.8	1.8	1.8

TABLE 2. Properties of the Porous Media.

Thickness (mm)	2	3	4
He II bath side (mm^2)	390.88	455.39	241.23
Test section side (mm^2)	392.87	455.12	251.77
Average Heat transfer Area (mm^2)	391.87	455.26	246.50

To achieve the temperature regulation of the He II bath, the pressure above the liquid surface is measured and held constant by a MKS Baratron® pressure sensor in combination with a pressure controller and a valve. The pressure sensor has an accuracy of ±0.25% of the reading and the pressure is controlled within ±0.02 Torr from 2.1 K to 1.4 K. The instrumentation components are a silicon piezo-resistive pressure sensor [3], two Allen Bradley (AB) carbon resistances, one located in the inner bath (Ti) and the other located in the bath cryostat (Tb) and a 30 Ω heater located in the inner bath. Thermometers are calibrated in situ before each experiment against the vapor pressure.

The steady-state temperature measurement of the inner bath is obtained using a lock-in amplifier (SR850 Stanford Research Systems). The AB thermometer of the inner bath is placed in a series with a large resistance and the feeding current is verified for each temperature. The temperature of the cryostat bath, Tb, is obtained with a four-wire technique with a DC battery current source. Tb is regulated within 1 mK and held constant for the entire range of power dissipation. The lock-in amplifier, used for temperature measurement, is connected to the power network through an insulation transformer in order to minimize electrical disturbances. The AB thermometer is placed in series with a 5 MΩ stable resistance at room temperature. The lock-in amplifier provides an AC voltage of 5 V rms at 5 Hz across the two resistances to obtain a feeding current through the AB thermometer of 1μA within 0.2% of accuracy. The feeding current is measured for each run. The electronic chain provides temperature measurement sensitivity within the range of ± 20 μK at 1.4 K and ± 200 μK at 2.0 K. The temperature difference error is at most 0.2 mK in the range of our investigation. This error analysis includes the resistance error measurement and the propagation error through the calibration curve. Total heat flux, is generated and monitored by a Keithley 2400 source meter and uncertainty is at most 0.5% of the value.

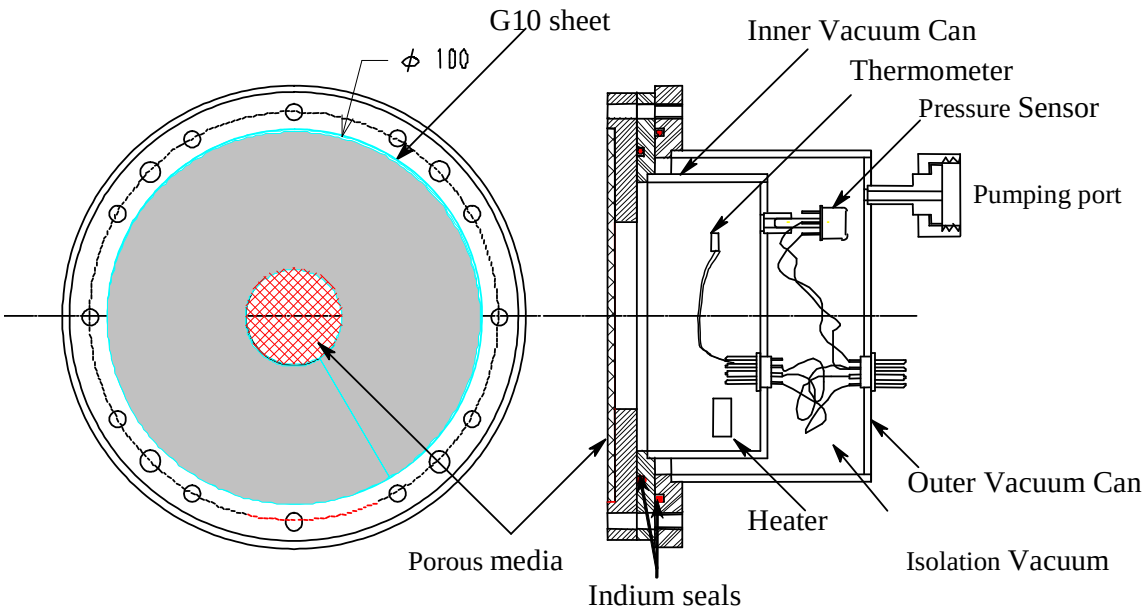

FIGURE 2. Schematic of the experimental set-up.

EXPERIMENTAL RESULTS AND ANALYSIS

General Description

The zero net mass flow regime is characterized by a null bulk mass density, $\rho_n|v_n|+\rho_s|v_s|=0$, which implies, in the phenomenological two-fluid model for He II, a counter-flow of normal and superfluid components. In the low velocity regime, analogous to a laminar regime for a classical Newtonian fluid, the pressure gradient is proportional to the temperature gradient, $\nabla p=\rho s \nabla T$, where ρ and s are the density and the entropy of helium. The heat flux q is related to the normal fluid velocity, v_n by $q=\rho s T v_n$. Equivalent to the laminar flow in the classical fluid, the Darcy law was found to be valid in the case of porous media [4]. The pressure gradient is given by,

$$\nabla p = \mu_n \frac{v_n}{K}, \tag{1}$$

where p is the pressure, μ_n is the viscosity of the normal component and K the permeability. This equation can be rewritten in terms of heat flux,

$$q = K \frac{(\rho s)^2 T}{\mu_n} \nabla T . \tag{2}$$

where s and ρ are entropy and density of the liquid, respectively. In the superfluid turbulent regime, it is observed that another dissipative force due to interactions between the two components of the liquid is induced. This force is assumed to be proportional to the cube of the relative velocity $F_{ns}=\rho_n\rho_s A(v_n-v_s)^3$, where A is the Gorter-Mellink coefficient. Assuming that the transition from laminar to turbulent is smooth, the temperature gradient is expressed for a porous media in the zero net mass flow regime as,

$$\nabla T = \frac{\mu_n}{K(\rho s)^2 T} q + \frac{A \rho_n}{s^4 \left(\rho_s T\right)^3} q^3 . \tag{3}$$

Permeability Determination

Measurements of the permeability, K, of the porous samples were carried out in He II. The measurement principle is based on the Darcy law where the macroscopic flow was steady and one dimensional. With the assumption of the isotropy of the porous media, and combining equation (1) and by $q=\rho s T v_n$ the pressure gradient is expressed as,

$$\nabla p = \mu_n \frac{v_n}{K} = \frac{1}{K} \frac{\mu_n}{\rho S T} q . \tag{4}$$

FIGURE 3 presents the results of the pressure difference across each sample Δp as a function of the heat flux q. One can see that there is a linear region corresponding to the laminar regime across the porous media where equation (4) is applied to determine the permeability. The measurements had been done for each sample and several temperatures.

TABLE 3. Permeability $\times 10^{14}$ (m^2)

Thickness (mm)	2	3	4
1.7 K	2.3	4.2	5.0
1.9 K	2.3	3.6	5.5
2.1 K	2.4	3.7	6.0

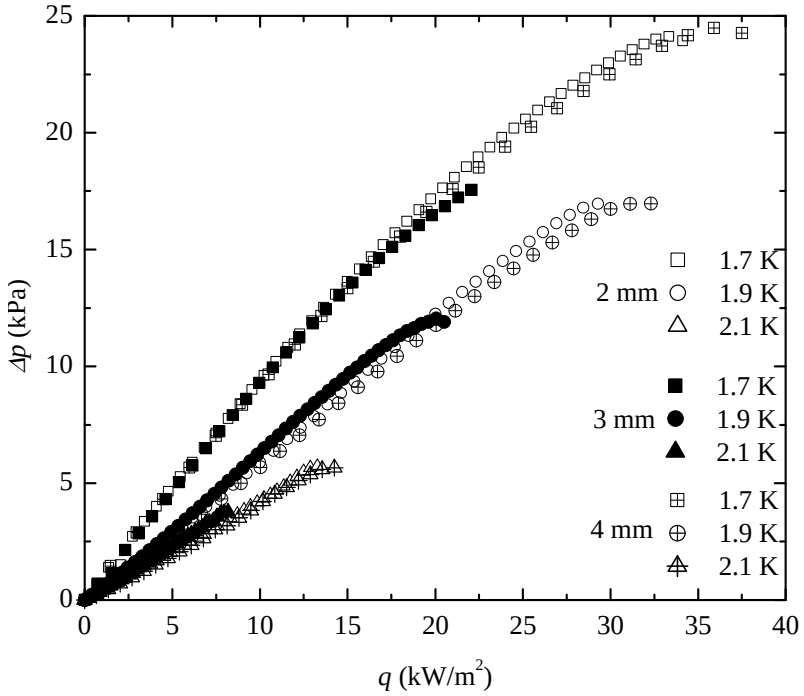

FIGURE 3. Pressure difference as a function of the bath temperature and sample thickness.

Results are presented in TABLE 3. The determination of the permeability is done for small value of Δp where the proportionality of Δp and q is in the linear region. The results of permeability indicate some discrepancies with the data given by Krosaki. Even though the permeability is merely a geometrical constant, the experimental results show higher value than their specification. It seems that the permeability values are somehow proportional to the thickness. In such a restricted geometry, the Darcy law may not be valid under the form of equation (4). As the permeability is a macroscopic parameter, one can imagine that K would increase as the thickness increases due to the increase of the flow paths. An average length of the flow path should be used in the pressure gradient in equation (4) instead of the physical overall thickness of the sample. In other words, the pressure gradient should be smaller if the sample is built with an average length of the flow path and therefore the effective permeability should be smaller than the one we found. Finally we can add that the accuracy on the determination of heat transfer areas can affect the permeability results. We do not know actually if the glue to attach the sample to the support flange penetrates the inside of porous media and how this effect modifies the heat transfer areas.

Temperature Difference Data

Laminar Regime

In laminar regime, equation (2) can be used to model the data. Because our ΔT range is important, the variation of the thermodynamical properties with the temperature has to be taken into account and the heat flux in laminar regime q_l is described by

$$q_l = \frac{K}{e}\int \frac{(\rho s)^2 T}{\mu_n} dT \ . \qquad (5)$$

where e is the physical thickness of the media. FIGURE 4 presents the comparison

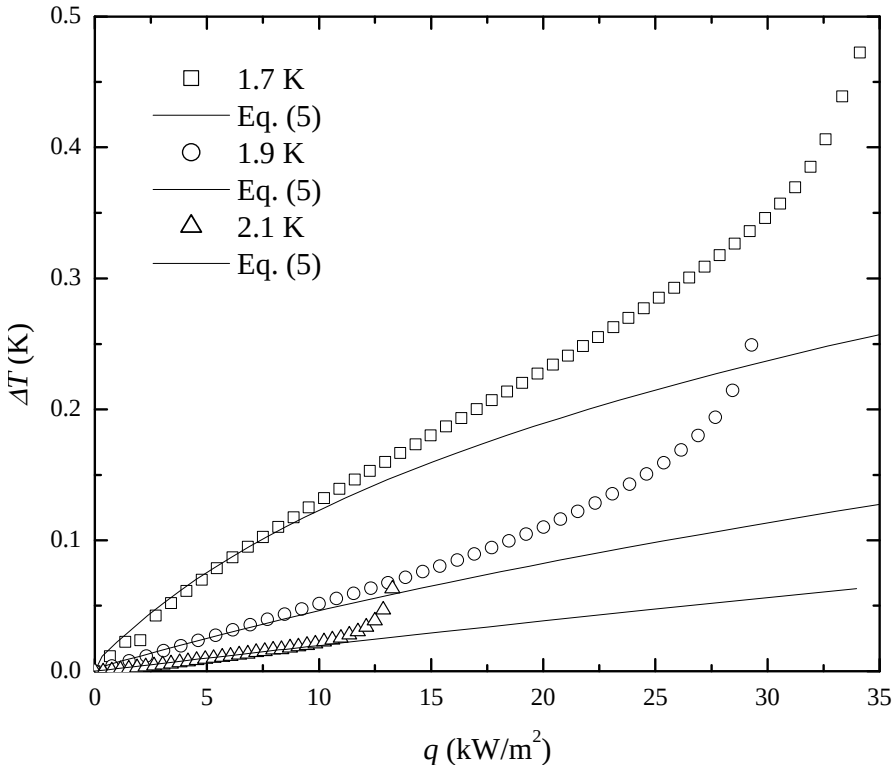

FIGURE 4. Temperature difference as a function of the bath temperature for the 2 mm thick sample and the comparison with equation (5).

between our results and equation (5) for the 2 mm thick sample. The calculation is done for each sample with the permeability determined in the previous section (TABLE 3). One can see clearly the transition from the laminar regime to the turbulent regime where an extra temperature difference is created due to the interaction between the normal and superfluid component. The results are well described by equation (5) for all samples and are independent of the thickness of the sample at low heat flux regime.

In the turbulent regime, for the same reasons, the heat flux, q_t, has to be calculated with integration,

$$q_t = \left(\frac{1}{e} \int \frac{s^4 (\rho_s T)^3}{A \rho_n} dT \right)^{1/3} . \tag{6}$$

According to equation (3), the temperature difference due to the laminar term, ΔT_l, given by equation (5) and the turbulent term, ΔT_t, given by equation (6) should be added to match our experimental results as,

$$\Delta T = \Delta T_l + \Delta T_t . \tag{7}$$

The comparison between this model and our measurements is displayed for the 2 mm thick sample in FIGURE 5 for three bath temperatures. Equation (7) is displayed as a solid line. FIGURE 5 presents a fair agreement between equation (7) and our data but the Gorter-Mellink law (equation (6)) has been modified. The Gorter-Mellink coefficient A(T) is considered as a fitting parameter to the experimental data. It is found that A(T) has to be multiplied by 20 for the 2 mm thick sample, while it needs to be multiplied by 10 for 4mm thick sample as shown in FIGURE 6. Our approach is based on the postulate that the

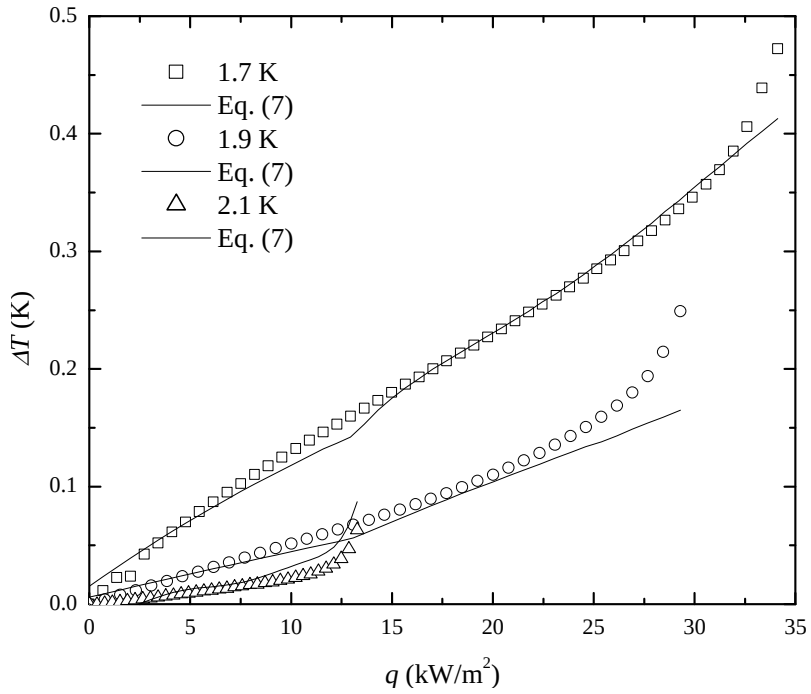

FIGURE 5. Temperature difference as a function of the bath temperature for the 2 mm thick sample and the comparison with equation (7).

interaction between the normal and the superfluid components in the mutual friction regime is higher in restricted geometry than the one in bulk helium, which results in the higher measured ΔT across the sample. Considering that the vortex lines are more concentrated in the pore of the media, one can imagine that the vortex line density is much higher than in the bulk helium. The over all effect increases the Gorter-Mellink coefficient, A(T). This picture assumes that the superfluid turbulence is still fully developed and can be modeled macroscopically by the Gorter-Mellink law.

Yuan demonstrates the same phenomenon for several porous media with permeability from 10^{-15} to 10^{-11} cm^2 [5]. It is proposed to use a modified Gorter-Mellink constant for porous media K_{GM}* as a function of the bulk one $K_{GM}=[\rho/(\rho_s\mu_n A(\mathrm{T}))]^{1/3}$,

$$K_{GM}* = \left[1/K_{GM}{}^2 + \left(10^{-7}/K\right)^2\right]^{-1/2}. \qquad (8)$$

If the definition of K_{GM}* is identical to K_{GM} then for a sample having the permeability and a permeability of 10^{-14} m^2, A(T) in their experiment is 10^6 higher than that of bulk helium. Maddocks presented also higher value of A(T) for porous media [6] in counter flow regime. The determined value of A(T) are 2 to 4 times larger than in the bulk helium. These results are in better agreement with our data and the A(T) coefficient is in the same order of magnitude.

This approach is certainly simplistic since in a restricted geometry the homogenous assumption of the superfluid turbulence may not be valid due to the non homogeneity of the geometry of such a media. In addition, the tortuosity of the media combined with possible flow restrictions of the flow path may create possible effect due to viscous interaction and path length. The latter effect might explain the difference of the Gorter-Mellink coefficients between the 2 and 4 mm thick sample. Validation of smooth transition from laminar to turbulent is required. Obviously more work should be done to investigate the effect of the sample thickness on the Darcy and mutual friction law and on the validity of the overall model.

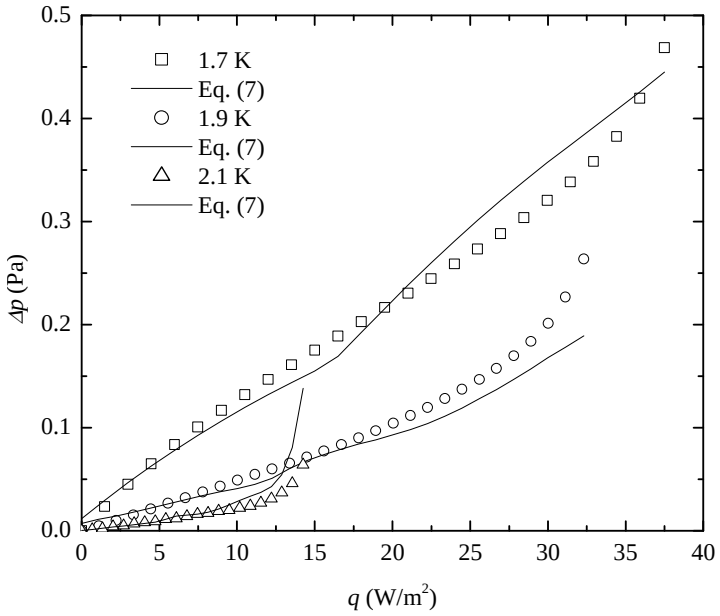

FIGURE 6. Temperature difference as a function of the bath temperature for the 4 mm thick sample and the comparison with equation (7).

CONCLUSION

Pressure and temperature difference measurement in counter flow regime through porous media show that in the laminar regime, the well-known Darcy law gives permeability with a dependency with the thickness of the sample. This effect might be due to a longer effective flow path depending on the thickness of the sample. It is shown that in the turbulent regime the temperature difference is the sum of the laminar term, ΔT_l, and the turbulent term due to mutual friction. To fit the data, the Gorter-Mellink coefficient A(T) is higher than in bulk helium and depends on the thickness of the sample.

ACKNOWLEDGMENTS

We would like to express our gratitude to Dr. T. Haruyama who kindly provides us pressure sensors for the experiment.

REFERENCES

1. J.A. Rice, P. E. F., C.S. Hazelton, "Mechanical and electrical properties of wrappable ceramic insulation," in *IEEE Trans. Applied Sup. ASC Proceedings* 9, 1999, pp. 220-223.
2. Meuris, C., *et al.*, *Cryogenics*, **39**, pp. 921-931, (1999).
3. Haruyama, T., *et al.*, "Silicon pressure sensor for in situ pressure measurement in a pressurized superfluid helium environment," in *Advances in Cryogenic Engineering* 43A, edited by P. Kittel, Plenum, New York, 1998, pp. 781-788.
4. Yuan, S. W. K. and Frederking, T. H. K., "Darcy Law of Thermo-Osmosis for Zero Net Mass Flow at Low Temperatures," in *ASME-JSME Thermal Engineering Conference*, 1983, pp. 191-197.
5. Yuan, S. W. K., "*The Non-Newtonian Heat and Mass Transport of He II in Porous Media Used for Vapor-Liquid Phase Separation*," U.C.L.A, Los Angeles, Ph.D. Dissertation 1985.
6. Maddocks, J. R. and Sciver, S. W. V., *Journal of Low Temperature Physics*, **96**, pp. 245-274, (1994).